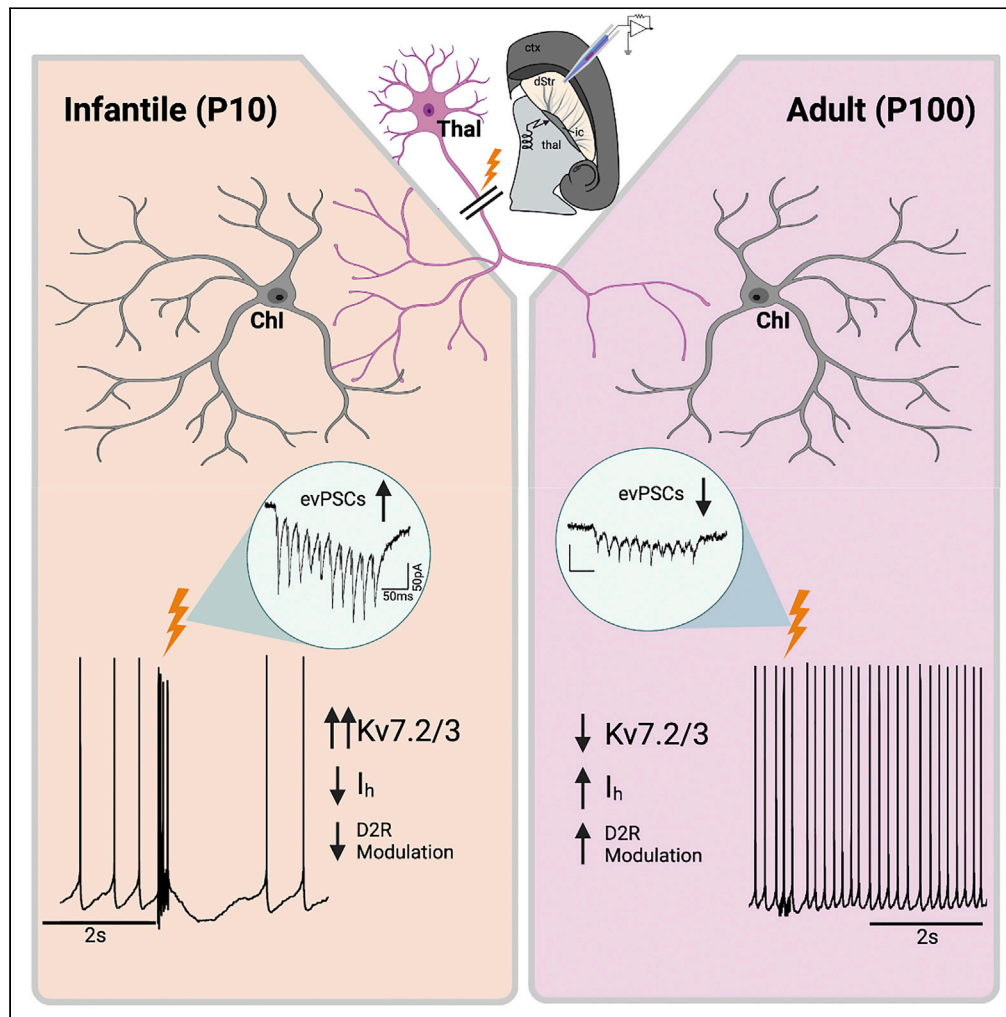


Article

Developmental regulation of thalamus-driven pauses in striatal cholinergic interneurons



Avery McGuirt,
Irena Pigulevskiy,
David Sulzer

afm2150@cumc.columbia.edu (A.M.)
ds43@cumc.columbia.edu (D.S.)

Highlights

Thalamus-driven Chi pauses are more pronounced in infantile (P10) mice

Thalamostriatal excitatory input to ChIs wanes postnatally

Chi pause modulation by dopamine and I_h arises after P10

Functional expression of Kv7.2/3 is enhanced at P10 and promotes Chi pauses

McGuirt et al., iScience 25, 105332
November 18, 2022 © 2022 The Author(s).
<https://doi.org/10.1016/j.isci.2022.105332>



Article

Developmental regulation of thalamus-driven pauses in striatal cholinergic interneurons

Avery McGuirt,^{1,*} Irena Pigulevskiy,¹ and David Sulzer^{1,2,*}

SUMMARY

In response to salient sensory cues, the tonically active striatal cholinergic interneuron (ChI) exhibits a characteristic synchronized “pause” thought to facilitate learning and the execution of motivated behavior. We report that thalamostriatal-driven ChI pauses are enhanced in *ex vivo* brain slices from infantile (P10) mice, with decreasing expression in preadolescent (P28) and adult (P100) mice concurrent with waning excitatory input to ChIs. Our data are consistent with previous reports that the adult ChI pause is dependent on dopamine signaling, but we find that the robust pausing at P10 is dopamine independent. Instead, elevated expression of the noninactivating delayed rectifier Kv7.2/3 current promotes pausing in infantile ChIs. Because this current decreases over development, a parallel increase in I_h further attenuates pause expression. These findings demonstrate that cell intrinsic and circuit mechanisms of ChI pause expression are developmentally determined and may underlie changes in learning properties as the nervous system matures.

INTRODUCTION

Rudimentary motivated behaviors are expressed from birth (Alleva and D’Udine, 1987; Hall et al., 1977), but infants respond to a limited subset of environmental cues with a limited set of actions (Bulut and Altman, 1974; Fox, 1965). As animals mature, a vast repertoire of motor programs is acquired and selectively recruited on confrontation with a growing set of subtly differentiable cues (Altman and Sudarshan, 1975).

As the input nucleus of the basal ganglia (BG), the striatum is critical for the learned transduction of environmental stimuli to appropriately controlled behavioral responses. It is predominantly composed of dopaminergic GABAergic spiny projection neurons (SPNs), which integrate a variety of inputs from higher brain regions, thalamus, and midbrain dopamine projections and send long-range projections to downstream BG targets (Gerfen and Surmeier, 2011). Locally, striatal acetylcholine (ACh) modulates dopamine release by activation of nicotinic acetylcholine receptors (nAChRs) on dopaminergic axons, as well as SPN excitability and excitation through stimulation of pre- and postsynaptic muscarinic and nicotinic receptors (Howe et al., 2016; Oldenburg and Ding, 2011; Rice and Cragg, 2004; Threlfell et al., 2012; Zhang and Sulzer, 2004). Thus, dopamine signaling and SPN activity are regulated by the activity of cholinergic interneurons (ChIs), a population of characteristically large, tonically active cells that comprise approximately 1–5% of striatal neurons (Bolam et al., 1984; Braak and Braak, 1982; Kemp and Powell, 1971).

ChIs exhibit a characteristic transient quiescence, or “pause” in firing, following the presentation of cues predictive of either appetitive or aversive stimuli (Aosaki et al., 1994b; Joshua et al., 2008). At the circuit level, ChIs are highly innervated by thalamic axons, whereas cortical inputs are sparse and largely targeted to the ChI’s distal dendrites (Lapper and Bolam, 1992; Smith et al., 2004). In both rodents and primates, input from the thalamus is particularly important for initiating the ChI pause (Ding et al., 2010; Matsumoto et al., 2001). In addition, pharmacological modulation and lesions of midbrain dopamine neurons suggest that the pause is partially dependent on activation of dopamine D2 receptors on the ChI (Aosaki et al., 1994a; Ding et al., 2010).

Attempts to isolate the cell-intrinsic mechanisms of the ChI pause have focused on afterhyperpolarizations induced by direct depolarizing current injections to individual ChIs (Oswald et al., 2009; Wilson, 2005; Zhang et al., 2018). These data suggest that inactivation of HCN channels and/or recruitment of outward potassium currents is responsible for pause generation. However, direct depolarization may not recruit

¹Departments of Psychiatry, Neurology, Pharmacology, Columbia University Irving Medical Center, Division of Molecular Therapeutics, New York State Psychiatric Institute, New York, NY 10032, USA

²Lead contact

*Correspondence: afm2150@cumc.columbia.edu (A.M.), ds43@cumc.columbia.edu (D.S.)

<https://doi.org/10.1016/j.isci.2022.105332>



the same set of conductances as endogenous synaptic innervation. Furthermore, these preparations would not be expected to elicit dopamine release and do not show robust dopamine modulation of the resultant pause-related hyperpolarizations.

We have previously shown that nigrostriatal dopamine release rapidly increases over the first four postnatal weeks in mouse brain slices (Lieberman et al., 2018) and that the intrinsic activity of ChIs is highly developmentally regulated, with a collection of ionic currents related to pacemaking in ChIs increasing over postnatal development (McGuirt et al., 2021). Here, we explore the postnatal development of the ChI in the context of the thalamostriatal circuit and probe whether the initiation and kinetics of the pause are developmentally determined during the period when learning and behavioral competencies rapidly mature in mice. Using a brain slice preparation that retains thalamostriatal projections (Ding et al., 2010; Smeal et al., 2007), we elicit pause responses in ChIs in the dorsal striatum by electrical stimulation of thalamostriatal afferents. We find that pause responses are most robust in infantile (P10) mice, and decrease with age concomitant with decreasing glutamatergic input. The pauses of infantile ChIs are independent of D2R signaling, as demonstrated by pharmacological D2R blockade. In contrast, the proportion of P28 and P100 ChIs showing thalamus-driven pause responses was significantly decreased following D2R blockade. Of interest, a developmental increase in I_h expression corresponds with decreasing pause responses, and I_h blockade in older animals promotes more robust pausing as seen at P10. Finally, we find that elevated functional expression of a slowly-activating, non-inactivating potassium current carried by Kv7.2/3 promotes pausing at P10, whereas blockade of this current had little effect at older ages. These data indicate that the thalamus-driven ChI pause is dependent on the coordinated expression of multiple biophysical mechanisms that are differentially recruited during postnatal development.

RESULTS

Thalamus-driven ChI pauses are enhanced in infantile mice

To assess responses of ChIs to thalamic innervation, we used a previously described striatal slice preparation that retains the integrity of thalamostriatal afferents (Figure 1A) (Ding et al., 2010). As expected, a significant subset of cells showed a significant pause in firing at the termination of electrical stimulation of thalamostriatal afferents (Figures 1B–1H). In preadolescent (P28) and adult (P100) mice, the length of this pause roughly matched the sub-second duration of pause responses in classic studies of behaving primates (Aosaki et al., 1994b, 1995). However, in infantile mice (P10), the pauses were significantly longer (Figures 1B and 1F). We previously reported that over this developmental time course, ChIs increase their autonomous firing frequency (McGuirt et al., 2021). A “pause score” (PS), or the quotient of the pause duration and average interspike interval in the pre-stimulus period, was calculated for each cell to normalize for individual differences in firing frequency (see STAR methods and Figure S1). We found that pause responses were significantly more robust at P10 even after normalizing to baseline firing frequency, suggesting that ChI responses to excitatory innervation are developmentally dynamic beyond their intrinsic mechanisms for tonic action potential regeneration. Moreover, 83% of the ChIs in this initial P10 dataset showed a significant pause response ($p < 0.05$, paired t-test of pre-versus post-stimulus intervals), whereas only 61 and 53% of cells recorded showed pause responses at P28 and P100, respectively. We conclude that thalamus-driven ChI pauses are exaggerated at P10. We sought through subsequent experiments to identify candidate factors underlying this developmental refinement of the ChI pause at the levels of the thalamostriatal circuit and cell intrinsic currents.

Excitatory inputs to ChIs wane with age

Although ChI pauses *in vivo* are known to occur at times without an initial burst, pauses and pause-related membrane dynamics are suggested to covary with the strength of incoming excitation (Aosaki et al., 1994b; Ding et al., 2010; Wilson, 2005). Along with enhanced expression of the pause, P10 mice showed significantly faster average firing in response to thalamic stimulus relative to baseline firing rates (Figures 1F–1H). To interrogate developmental changes in the efficacy of the thalamostriatal stimulation paradigm, we quantified postsynaptic responses to the train stimuli used to evoke ChI pauses. Representative traces (Figure 2A) show the rapid development of a transient inward current after each stimulus pulse. By quantifying the amplitudes of the currents evoked by the first stimulus pulse (evPSCs), a decrease in the strength of this thalamic input was revealed over postnatal development (Figure 2B). An additional set of cells was given paired thalamic stimuli at 20 Hz to assay potential differences in short term plasticity while mitigating the potential confound of current accumulation at 50 Hz. Although a previous study using 10 Hz stimulation showed paired pulse facilitation of thalamic inputs onto ChIs in adult mice, our protocol elicited

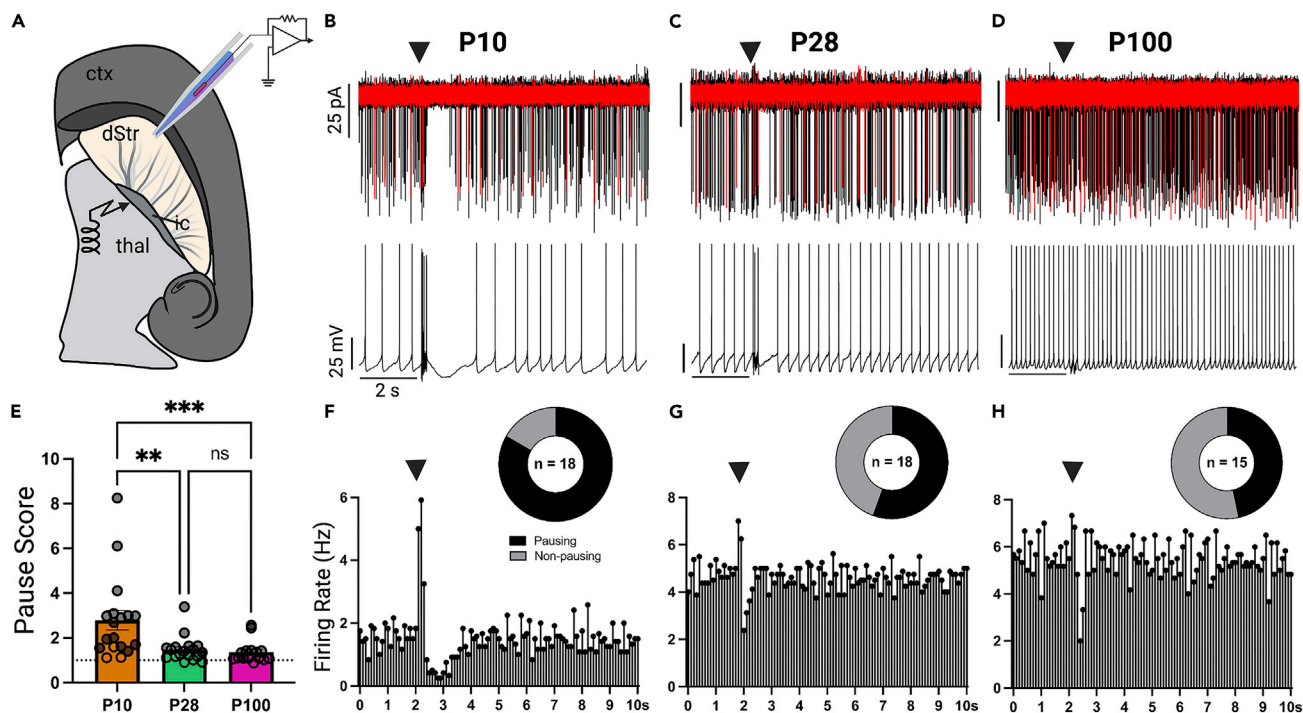


Figure 1. Postnatal reduction in the thalamus-evoked Chl pause

(A) Schematic of ex vivo angled horizontal slice configuration. ctx = cortex; dStr = dorsal striatum; ic = internal capsule; thal = thalamus. (B–D) Representative cell-attached (top) and whole cell current-clamp (bottom) recordings of ChIs in P10, P28, and P100 mice in response to train stimulation of thalamic afferents. Ten consecutive cell-attached traces (top) were averaged for each cell for pause analysis in (E). (E) Summary of age effect on normalized pause length (pause score, or PS). See Figure S1 for explanation of pause quantification. Results analyzed by Kruskal-Wallis analysis of variance (ANOVA) (K-W) followed by Dunn’s multiple comparison test. K-W p 0.0002; K-W statistic = 16.93. Dunn’s mean rank differences (denoted on figure): P10 vs. P28 adjusted p 0.0080; P10 vs. P100 p = 0.0003; P28 vs. P100 p = 0.896. P10 n = 18 cells (3 mice), P28 n = 18(4), P100 n = 15(6). Error bars denote SEM. Shaded circles represent cells exhibiting significant pause responses. (F–H) Summary peristimulus time histograms (PSTHs) for all significantly pausing cells in (E). Pie charts (inset) show proportion of cells in (E) exhibiting significant pause responses.

no significant plasticity at P28 or P100 and a small level of facilitation at P10 (Figure 2C) (Tanimura et al., 2016). The distributions of paired pulse ratios did not significantly differ with age, however, suggesting no significant change in release probability consistent with the developmentally decreasing strength of thalamic input.

Evoked postsynaptic responses were then correlated with the pause responses initially measured from these cells. At P10, when evPSCs were the largest, there was no significant correlation between evPSC amplitude and PS (Figure 2D). In contrast, at older ages, we found a significant positive correlation between the magnitude of evPSCs and PS evoked in ChIs (Figure 2E). This suggests a saturation of pause responses at P10 due to robust innervation by the thalamus, whereas at P28 and P100 the relatively weaker thalamic innervation results in a portion of the variance in pause response being determined by variability in thalamic input strength.

To further elucidate the observed decrease in excitatory input strength, we recorded miniature excitatory postsynaptic currents (mEPSCs) from a group of ChIs in the DLS at the same ages. Although this nonbiased approach captures all excitatory inputs (i.e., not only from the thalamus), comparing properties of the mEPSCs can provide evidence of a pre or postsynaptic origin of this developmental change. Further, the thalamus exerts predominant excitatory control over ChIs compared to other sources (Lapper and Bolam, 1992; Smith et al., 2004), so we hypothesized that P10 ChIs would show stronger glutamatergic innervation compared with older ages even in this nonspecific assay. Indeed, the overall frequency of mEPSCs decreased significantly with age with roughly half of the cells recorded at P100 showing no identifiable events (Figure 3A). When comparing cells that exhibited multiple identifiable events, there was a significant

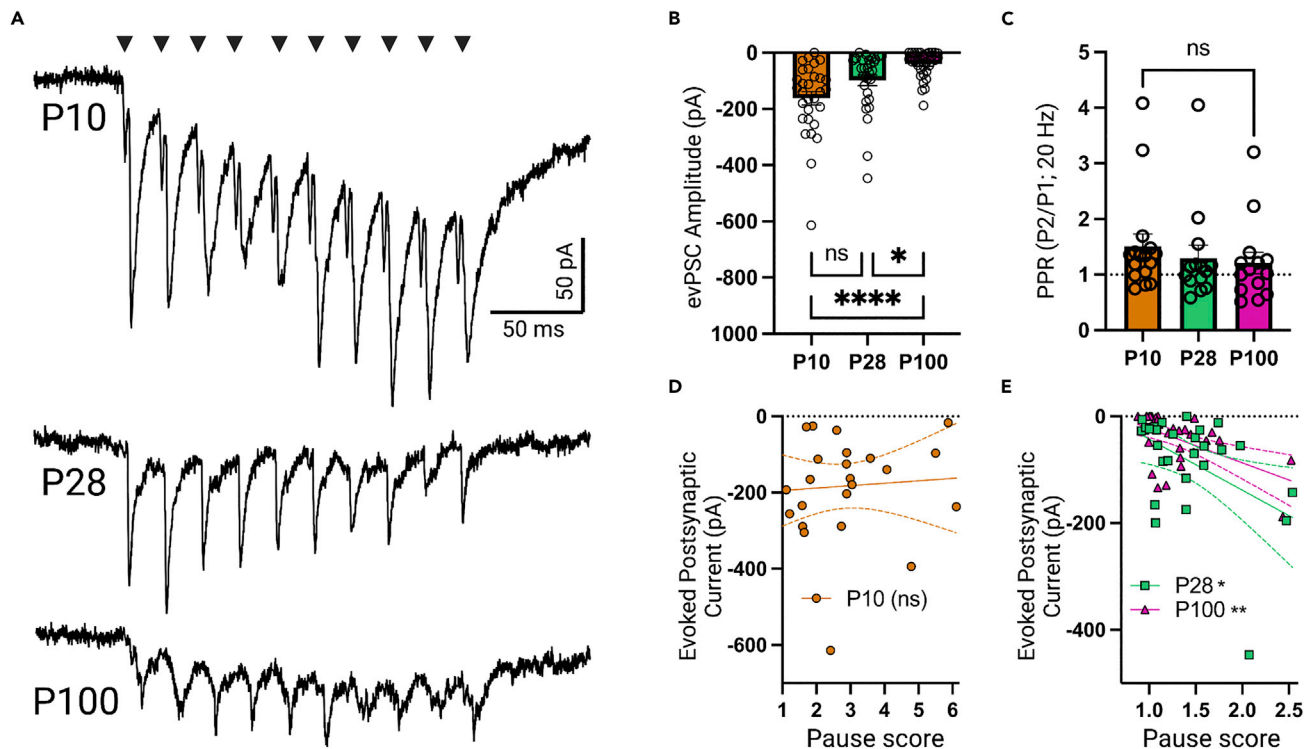


Figure 2. Postnatal reduction in thalamus-evoked postsynaptic currents

(A) Representative voltage-clamp (holding potential -60 mV) traces of transient inward currents evoked by train stimulation of thalamic afferents (evPSCs). Arrowheads denote stimulus pulse onset. Stimulus artifacts (1 ms each) removed for clarity.

(B) Summary of age effect on initial evPSC. Each datapoint represents a single cell, for which the amplitude of the current evoked by the first stimulus pulse was averaged for three consecutive sweeps. Data analyzed by K-W test followed by Dunn's multiple comparison test. K-W $p < 0.0001$; K-W statistic = 26.16. Dunn's mean rank differences (denoted on figure): P10 vs. P28 adjusted $p = 0.0565$; P10 vs. P100 $p < 0.0001$; P28 vs. P100 $p = 0.0219$. P10 $n = 31$ cells (10 mice), P28: $n = 30$ (11), P100: $n = 34$ (15).

(C) evPSC paired pulse ratios (PPR) in a separate set of cells stimulated at 20 Hz. Ages compared by one-way ANOVA: $p = 0.599$. Each age distribution compared to hypothetical value of PPR = 1 via one sample t-test: P10 $p = 0.0376$; P28 $p = 0.222$; P100 $p = 0.299$.

(D and E) Correlation between evPSC amplitude in (B) and PS in ChIs from P10 (D), P28, and P100 (E). Linear regressions: P10 $R^2 = 0.00492$, $p = 0.745$; P28 $R^2 = 0.204$, $p = 0.0181$; P100 $R^2 = 0.281$, $p = 0.0013$. Data in (B–E) combine cells from the dataset in Figure 1 with controls from experiments in Figures 4A and 5C.

shift in the cumulative distributions of interevent intervals toward lower-frequency (longer interval) events between P28 and P100 (Figure 3C). There was, however, no change in the average amplitudes of mEPSCs (Figure 3B), suggesting a primarily presynaptic developmental change. Given the lack of strong evidence for a change in release probability that would be consistent with our observations (see above); these data point toward a reduction in the number of thalamus-ChI synapses over maturation.

Dopamine dependence of the ChI pause is developmentally determined

In both *in vivo* and reduced preparations, the ChI pause and related ChI membrane dynamics are mediated by dopamine signaling through D2 dopamine receptors (D2Rs) (Aosaki et al., 1994a; Ding et al., 2010; Kharkwal et al., 2016; Sanchez et al., 2011). We previously showed that evoked dopamine release and tyrosine hydroxylase expression in striatal slices increases rapidly over the early postnatal period, and that cholinergic modulation of dopamine release is highly developmentally dynamic (Lieberman et al., 2018; McGuirt et al., 2021). We sought to determine the dopamine-dependence of the ChI pause in this preparation and whether the exaggerated pauses observed at P10 were mediated by D2R signaling.

We probed the D2R-dependence of the ChI pause by recording pause responses in slices incubated with the D2R antagonist sulpiride (10 μ M), alternated with vehicle-incubated slices (Figure 4A). Strikingly, there was no difference between the pause responses or proportion of significantly pausing cells at P10 after sulpiride incubation (86 and 83% of cells paused in controls and sulpiride-incubated cells, respectively), suggesting that these robust pause responses are independent of D2R activation. At older

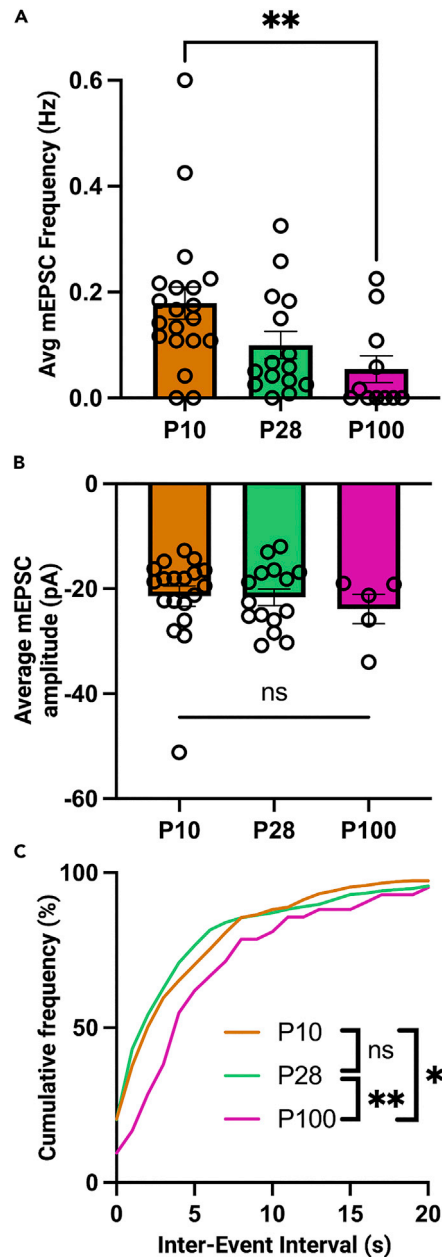


Figure 3. Excitatory inputs to ChIs decrease postnatally

(A) Average frequency of miniature excitatory postsynaptic currents (mEPSCs) recorded in ChIs in the DLS. mEPSCs were recorded in the presence of tetrodotoxin (TTX, 1 μ M) and picrotoxin (PTX) (50 μ M) for 2 min per cell. Data analyzed by K-W ANOVA followed by Dunn's multiple comparison test. K-W $p = 0.0093$; K-W statistic = 9.351. Dunn's mean rank differences (denoted on figure): P10 vs. P28 $p = 0.296$; P10 vs. P100 $p = 0.0077$; P28 vs. P100 $p = 0.460$. P10 $n = 20$ cells (4 mice); P28 $n = 15$ (4); P100 $n = 11$ (4).

(B) Average amplitude of mEPSCs in (A). Data analyzed by one-way ANOVA followed by Bonferroni correction: $F(2,36) = 0.0417$, $p = 0.959$; all individual comparisons $p > 0.999$.

(C) Cumulative distribution of mEPSC interevent intervals in cells from (A) with ≥ 2 identified events. Distributions compared by Kolmogorov-Smirnov tests. P10 vs. P28 $p = 0.282$, $D = 0.0787$; P10 vs. P100 $p = 0.0135$, $D = 0.256$; P28 vs. P100 $p = 0.0046$, $D = 0.290$.

ages, although the PS distributions were not significantly different ($p = 0.25$ and 0.099 for P28 and P100, respectively), 26 and 0% of P28 and P100 cells showed significant pause responses following sulpiride incubation versus 64 and 43% in controls ($p = 0.03$ and 0.007 for P28 and P100, chi-square analysis). These

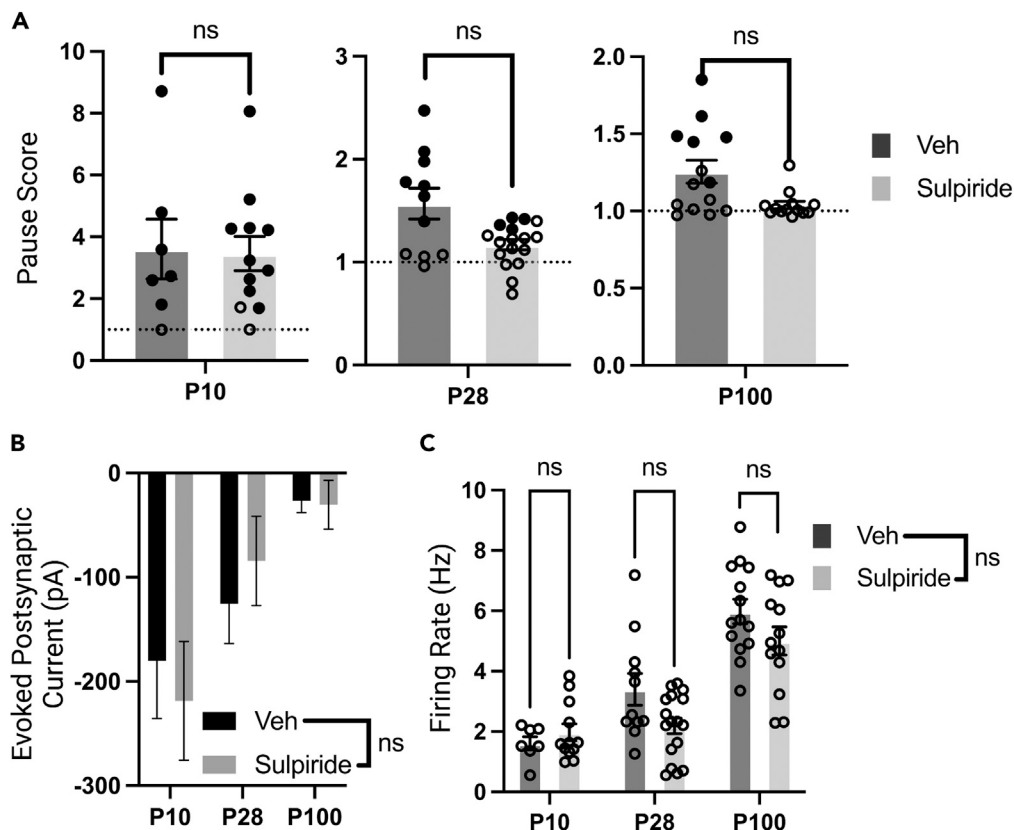


Figure 4. D2R-dependence of the ChI pause is developmentally determined

(A) Summary comparison of pause responses in cells incubated with D2 antagonist sulpiride (10 μ M) or vehicle (1:5000 DMSO). Pairs of samples analyzed by Mann-Whitney U tests followed by correction for multiple comparisons using the Bonferroni-Dunn method. P10 $p > 0.9999$, $U = 41$; P28 $p = 0.245$, $U = 56$; P100 $p = 0.0995$, $U = 47$. P10 $n = 14$ cells (veh), 13 cells (sulpiride), (3 mice); P28 $n = 12$, 17 (3); P100 $n = 14$, 13 (4). Dotted lines represent PS = 1. Filled circles represent cells with significant pause responses. Proportion of pausing cells (veh, sulp; χ^2 pvalue): P10 (86%, 83%; 0.891); P28 (64%, 24%; 0.0338); P100 (43%, 0%; 0.0074).

(B) Comparison of evPSC amplitudes recorded in subset of vehicle versus sulpiride treated cells. P10 $p > 0.999$, $U = 34$, $n = 6$, 12 (3); P28 $p = 0.193$, $U = 54$, $n = 11$, 17 (3); P100 $p > 0.999$, $U = 61$, $n = 12$, 12 (4).

(C) Average basal firing rates of ChIs incubated in vehicle versus sulpiride. Data analyzed by two-way ANOVA with Bonferroni's multiple comparisons test: age \times drug $F(2, 68) = 1.989$, $p = 0.145$; age $F(2, 68) = 46.96$, $p < 0.0001$; drug $F(1, 68) = 3.482$, $p = 0.0663$. P10 vehicle versus sulpiride $p > 0.9999$; P28 $p = 0.0703$; P100 $p = 0.194$.

findings are consistent with previous reports of the role of signaling through D2R in facilitating the ChI pause. Importantly, these effects cannot be explained by D2-mediated changes in thalamic excitation or baseline membrane dynamics, as evPSCs and tonic firing rates were unchanged by sulpiride incubation (Figures 4B and 4C).

Developmental increase in I_h expression attenuates the ChI pause

The striatal ChI expresses a robust I_h current that we have shown increases between P10 and P100 (McGuirt et al., 2021). I_h has been suggested to be important for the generation and the kinetics of the ChI pause, although the mechanisms involved remain controversial and have largely been studied in the context of cell-intrinsic membrane dynamics rather than circuit-driven ChI pauses (Oswald et al., 2009; Zhang and Cragg, 2017; Zhang et al., 2018). We first sought to determine whether individual variation in ChI pause responses was explained by variation in functional expression of the I_h current. However, we found no significant correlation between I_h expression and PS at any age tested (Figure 5A). We then tested whether selective blockade of I_h with the HCN blocker ZD7288 (ZD, 1 μ M) altered expression of the ChI pause during postnatal development. ZD significantly increased pause expression at P28 and P100, but had no significant effect at P10 (Figure 5C). Consistent with our previous data (McGuirt et al., 2021), 1 μ M ZD incubation

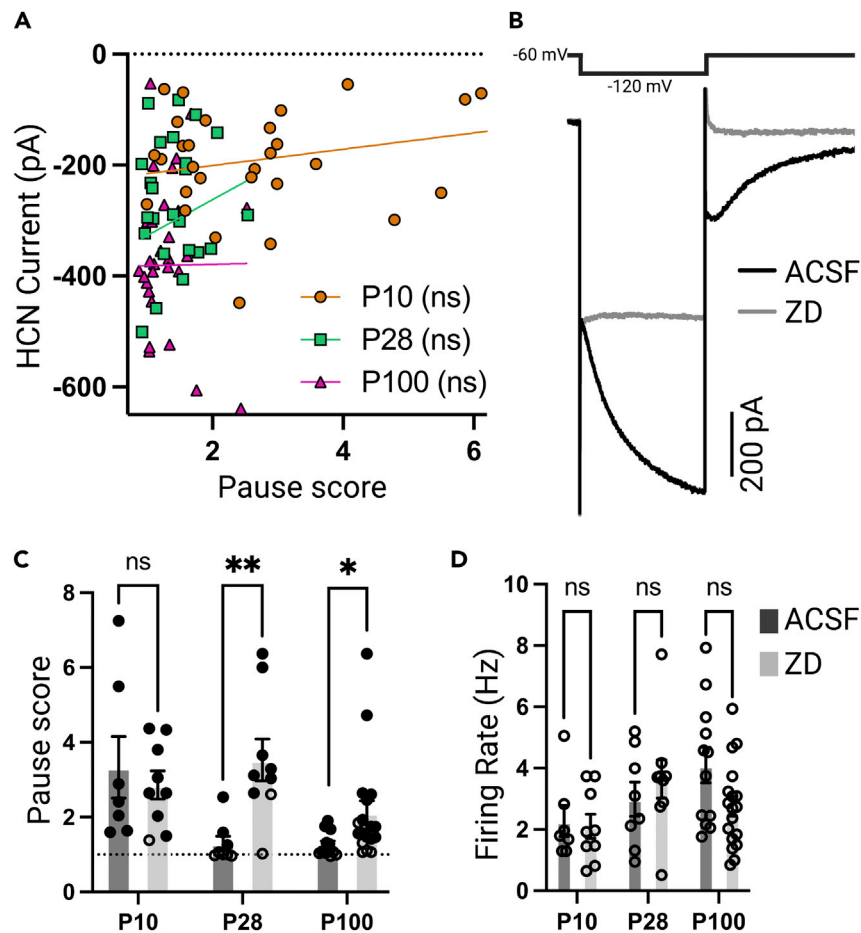


Figure 5. Developmental increase in I_h expression in ChIs contributes to postnatal reductions in pause length

(A) Correlations between HCN current magnitude and PS at P10, P28, and P100. Current calculated as difference between instantaneous and steady-state current following -60 mV hyperpolarizing voltage step from -60 mV holding potential (see B). Linear regressions: P10 $R^2 = 0.0887$, $p = 0.104$, $n = 31(10)$; P28 $R^2 = 0.0248$, $p = 0.442$, $n = 29(11)$; P100 $R^2 < 0.0001$, $p = 0.972$, $n = 31(15)$.

(B) Sample voltage-clamp trace shows I_h current evoked by hyperpolarizing step. I_h is abolished by superfusion of HCN blocker ZD7288 (ZD) ($1 \mu\text{M}$).

(C) Pre-incubation in ZD ($1 \mu\text{M}$) increases PSs at P28 and P100 but has no effect at P10. Pairs of samples were analyzed by Mann-Whitney U tests followed by correction for multiple comparisons using the Bonferroni-Dunn method. P10 corrected $p > 0.9999$, $U = 30$; P28 $p = 0.00296$, $U = 4$; P100 $p = 0.0200$, $U = 45$. P10 $n = 7$ cells (ACSF), 9 cells (ZD), (4 mice); P28 $n = 8, 9$ (4); P100 $n = 13, 16$ (5). Dotted line represents PS = 1. Filled circles represent cells with significant pause responses.

Proportion of pausing cells (veh, ZD; χ^2 p value): P10 (100%, 89%; 0.362); P28 (38%, 78%; 0.0921); P100 (55%, 72%; 0.331). (D) Average basal firing rates of ChIs incubated in vehicle versus ZD. Data analyzed by two-way ANOVA with Bonferroni's multiple comparisons test: age \times drug $F(2, 57) = 2.238$, $p = 0.116$; age $F(2, 57) = 3.344$, $p = 0.0423$; drug $F(1, 57) = 0.464$, $p = 0.499$. P10 vehicle versus ZD $p > 0.999$; P28 $p > 0.999$; P100 $p = 0.0799$.

resulted in complete I_h blockade (Figure 5B) with no effect on basal firing rate at any age (Figure 5D). These results suggest that as I_h expression increases postnatally, it acquires a role in regulating the expression of the ChI pause, perhaps by terminating the period of quiescence after stimulation.

Pauses at P10 are not mediated by the ChI's slow afterhyperpolarization

Striatal ChIs express a slow afterhyperpolarization (sAHP) that is prominent following exogenous depolarization and during rhythmic bursting (Goldberg and Wilson, 2005; Wilson and Goldberg, 2006). Due to its recruitment following driven depolarization, the sAHP has been proposed as a candidate mechanism for initiating ChI pause responses. We have previously shown that the amplitude of the sAHP is not age-dependent (McGuirt et al., 2021), but sought to uncover whether the enhanced P10 pauses we observed

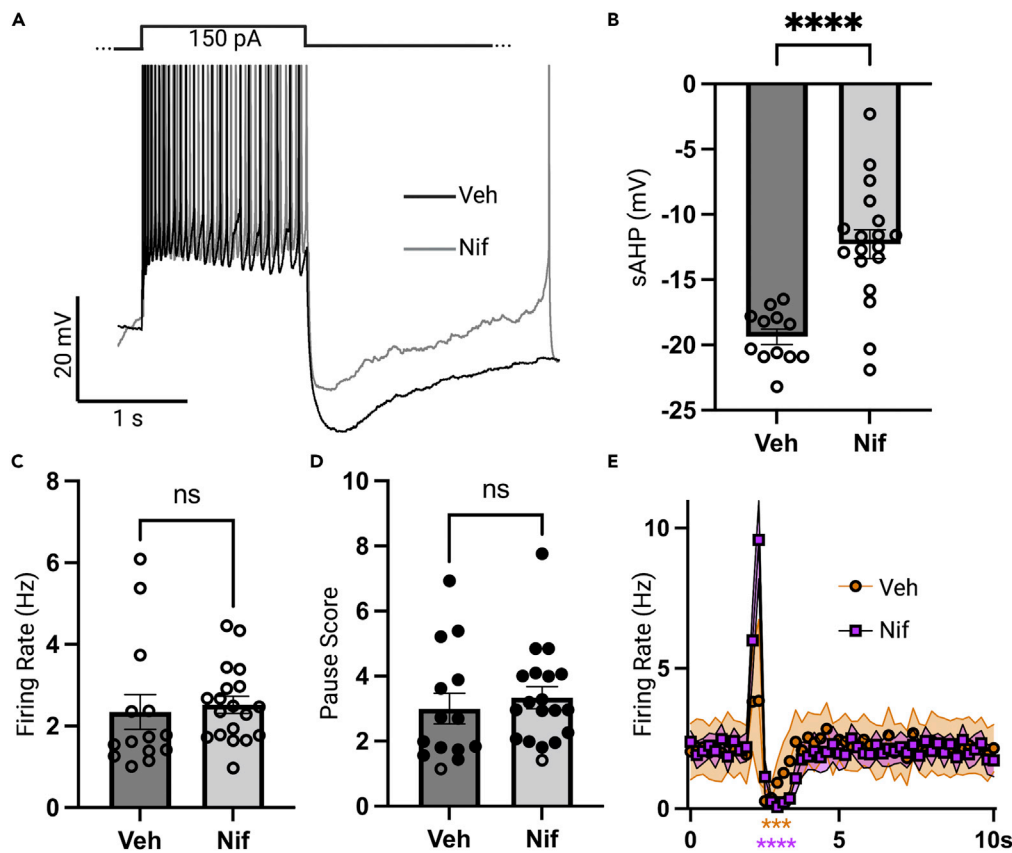


Figure 6. P10 Chl pauses are not mediated by the sAHP

(A) Sample whole cell current-clamp recordings of slow afterhyperpolarizations (sAHP) in P10 ChIs incubated in vehicle or nifedipine (nif, 20 μ M) following a 150 pA depolarizing current injection (bottom). Action potentials truncated.

(B) Comparison of sAHP magnitudes following vehicle or nifedipine incubation. Local minimum following current injection subtracted from baseline before current injection. Data analyzed by unpaired t-test: $p < 0.0001$; Veh $n = 12$ cells (4 mice); nif $n = 18$ (3).

(C) Comparison of baseline firing rates. Data analyzed by unpaired t-test: $p = 0.689$; veh $n = 14$ (4); nif $n = 19$ (3).

(D) Comparison of PSs following thalamic stimulation in ChIs incubated with vehicle or nifedipine. Data analyzed by Mann-Whitney test: $p = 0.240$; $U = 100$; veh $n = 14$ (4); nif $n = 19$ (3). Proportion of pausing cells (veh, nif; χ^2 p value) = (93%, 95%; 0.823).

(E) Summary PSTHs for all cells from (D). Each point represents a 200 ms bin and shading represents the 95% CI. Data analyzed by two-way repeated measures ANOVA with Bonferroni's multiple comparison test versus the final bin before stimulation (1.8s). Significance denoted on the figure refers to the 2.8s bin: veh $p = 0.0007$; nif $p < 0.0001$.

were nevertheless mediated by the sAHP. The sAHP is selectively coupled to L-type calcium channels, and is thus sensitive to dihydropyridines (Goldberg and Wilson, 2005). In P10 ChIs, nifedipine significantly reduced the expression of the sAHP, while having no effect on basal firing rates (Figures 6B and 6C). Despite downregulating sAHP expression, nifedipine had no effect on pause responses in P10 ChIs, suggesting that their robust pauses are independent of this conductance (Figures 6D and 6E).

Elevated expression of Kv7.2/3 current promotes enhanced Chl pauses at P10

Among striatal neurons, ChIs show the highest expression of the Kv7.2 and Kv7.3 channels that carry a slowly-activating, noninactivating potassium current (Saunders et al., 2018; Wang et al., 1998). Like the sAHP, this potassium current is recruited by significant exogenous depolarization, and has been recently suggested as a candidate mechanism for driving Chl pauses (Zhang et al., 2018). Depolarizing current injections from a hyperpolarized holding potential where Kv7.2/3 channels are inactive elicit a slowly-activating outward current that is sensitive to the Kv7.2/3 antagonist XE-991 (XE) (Figure 7A) (Shen et al., 2005). We found that this activation current was significantly higher in ChIs at P10 than at

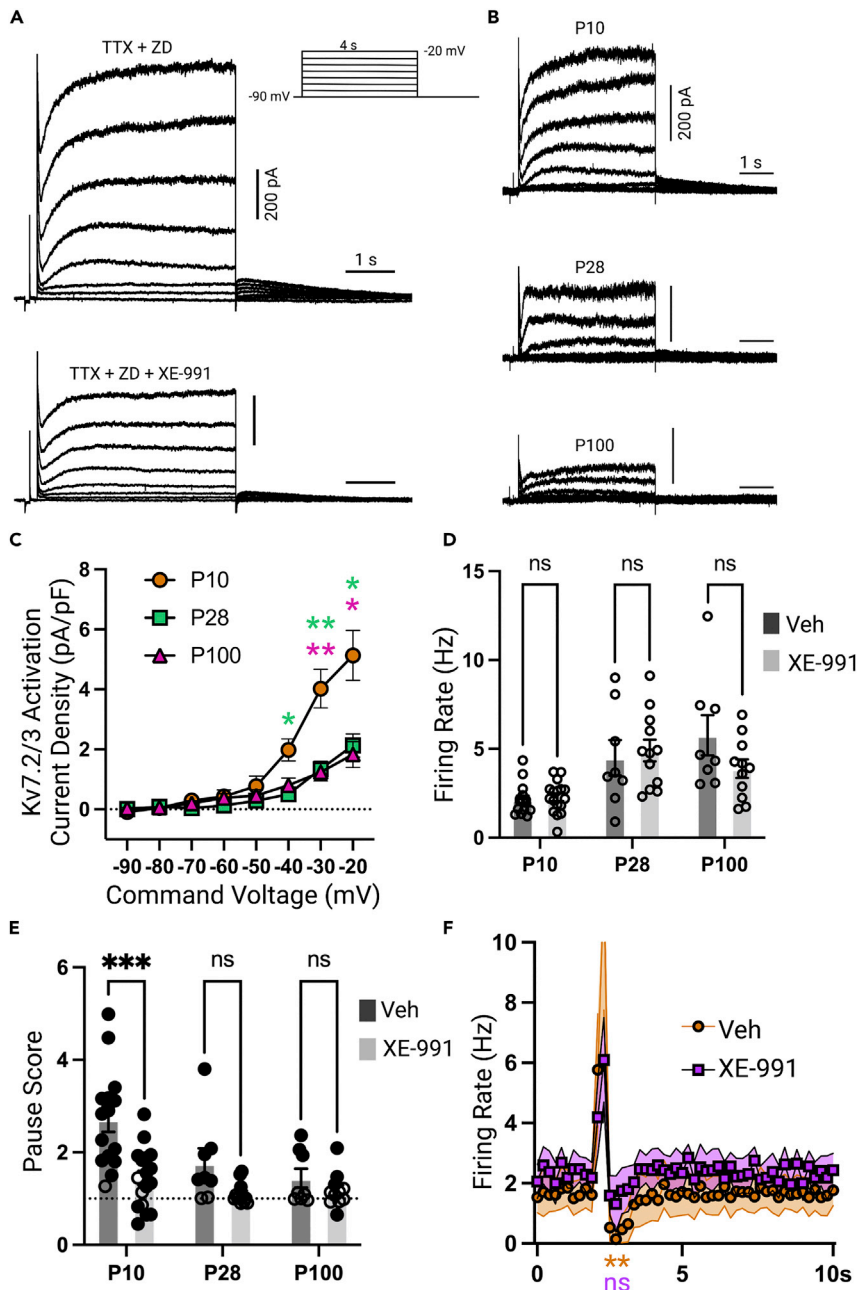


Figure 7. Elevated functional expression of the Kv7.2/3 potassium current facilitates pausing at P10

(A) Representative whole cell voltage-clamp recordings of ChIs during a protocol to elicit activation of the Kv7.2/3 current. Top, control condition with TTX (1 μ M) to block cell firing and ZD (1 μ M) applied to avoid confounding inactivation of HCN currents. Bottom, after additional application of XE-991 (XE, 25 μ M) to block Kv7.2/3 currents.

(B) Representative subtractions of voltage-clamp recordings before and after application of XE.

(C) Summary quantification of current-voltage dependence in XE-subtracted recordings of Kv7.2/3 activation current, normalized to cell capacitance. Data analyzed with two-way repeated measures ANOVA followed by Bonferroni correction. Voltage \times age $F(14, 182) = 10.73, p < 0.0001$; voltage $F(1.459, 37.93) = 72.53, p < 0.0001$; age $F(2, 26) = 8.296, p = 0.0016$. P10 $n = 9$ cells (5 mice); P28 $n = 9$ (4); P100 $n = 11$ (4).

(D) Average basal firing rates of ChIs incubated in vehicle versus XE. Data analyzed by two-way ANOVA with Bonferroni's multiple comparisons test: age \times drug $F(2, 65) = 2.196, p = 0.119$; age $F(2, 65) = 46.96, p < 0.0001$; drug $F(1, 65) = 0.947, p = 0.334$. P10 vehicle vs. XE $p > 0.999$; P28 $p > 0.999$; P100 $p = 0.103$.

(E) Pre-incubation in XE-991 decreases PSs significantly at P10 but has no significant effect at P28 or P100. Pairs of samples were analyzed by Mann-Whitney U tests followed by correction for multiple comparisons using the Bonferroni-Dunn

Figure 7. Continued

method. P10 corrected $p = 0.00124$, $U = 38$; P28 $p = 0.0757$, $U = 19$; P100 $p > 0.999$, $U = 36$. P10 $n = 15$ cells (veh), 17 cells (XE), (5 mice); P28 $n = 8$, 12 (4); P100 $n = 7$, 12 (4). Dotted line represents $PS = 1$. Filled circles denote cells with significant post-stimulation deviations from basal firing rate. Proportion of pausing cells (veh, XE; χ^2 p value): P10 (93%, 59%; 0.0245); P28 (75%, 67%; 0.690); P100 (43%, 25%; 0.419).

(F) Summary PSTHs for all P10 cells from (E). Each point represents a 200 ms bin, and shading represents the 95% CI. Data analyzed by two-way repeated measures ANOVA with Bonferroni's multiple comparison test versus the final bin before stimulation (1.8s). Significance denoted on the figure refers to the 2.8s bin: veh $p = 0.004$; XE $p > 0.999$.

P28 or P100, suggesting a rapid postnatal reduction in current expression during the first four postnatal weeks (Figures 7B and 7C).

We next assayed pause responses in cells incubated with XE to determine whether the Kv7.2/3 current facilitates pausing initiated by thalamic innervation. Although no significant differences were observed in the pause responses or proportion of pausing cells at P28 or P100, the XE group showed significantly reduced PSs at P10 (Figure 7E). Several cells even showed significant persistent excitatory responses beyond the termination of the stimulus (i.e., $PS < 1$). A collection of whole cell current-clamp recordings illustrating these responses at P10 in the control and XE conditions are shown in Figure S3. These data are consistent with the conclusion that Kv7.2/3 expression at P10 is particularly important for the enhanced expression of ChI pause responses that we observe.

Finally, to further characterize the postnatal development of Kv7.2/3-driven membrane dynamics, we applied a ramping depolarizing current injection protocol previously shown to selectively recruit a Kv7.2/3-mediated afterhyperpolarization (Zhang et al., 2018). Following this cell-intrinsic depolarization, an extended period of quiescence was observed in P10 ChIs (Figures 8A and 8B). P28 and P100 ChIs, in contrast, showed a significant but shorter duration decrease in firing rate, rather than complete quiescence, following cessation of the stimulus (Figures 8A and 8B). To isolate the Kv7.2/3-driven hyperpolarization, tetrodotoxin (TTX) was bath-applied before stimulation of ChIs with the ramping current injection to block cell firing. As expected, this hyperpolarization was blocked by application of XE (Figure 8C). Hyperpolarizations were normalized to the amplitude of the depolarization evoked by the stimulus, as previously reported (Zhang et al., 2018). We observed a significant decrease in the expression of the hyperpolarization over postnatal development with its normalized amplitude decreased by roughly half between P10 and P100 (Figure 8D). In combination with the current quantification and XE effects on pausing at P10, these data further support the conclusion that ChI pauses at P10 are facilitated by the enhanced functional expression of Kv7.2/3 currents, which then decrease postnatally.

DISCUSSION

Recent studies have illuminated the postnatal development of ChI intrinsic physiology, ACh-dopamine interactions, and striatal projection system input-output characteristics (Khandelwal et al., 2021; Kozorovitskiy et al., 2012, 2015; Lieberman et al., 2018, 2020; McGuirt et al., 2021; Peixoto et al., 2016, 2019). Here, we have investigated the maturation of the ChI pause, a circuit-driven phenomenon thought to be related to cue learning, behavioral flexibility, and attention. Using an acute slice preparation that allows controlled access to thalamostriatal afferents with electrophysiological recordings of individual ChIs, we identified significant changes in the ability of the thalamostriatal circuit to drive firing dynamics in ChIs and the responses of ChIs to incoming excitation. We find that the most significant change in pausing responses occur between P10 and P28, a period when mice rapidly expand their behavioral repertoire and acquire the ability to respond to a growing set of learned environmental cues.

Maturation of the ChI pause

Here, we show that the ChI pause driven by thalamostriatal excitation is far more robust in infantile (P10) than preadolescent (P28) or adult (P100) mice. ChI quiescence at P10 following thalamostriatal stimulation often lasts for multiple seconds, far longer than the baseline interval between spontaneous action potentials. Furthermore, although a large majority of ChIs recorded at P10 exhibited obvious and robust pausing responses, ChI pauses at older ages were only observed in a fraction of cells. Similar developmental differences were observed in pauses evoked by cell-intrinsic depolarizing current injections, indicating that both the circuit-level and cell-intrinsic mechanisms for pause generation are developmentally regulated.

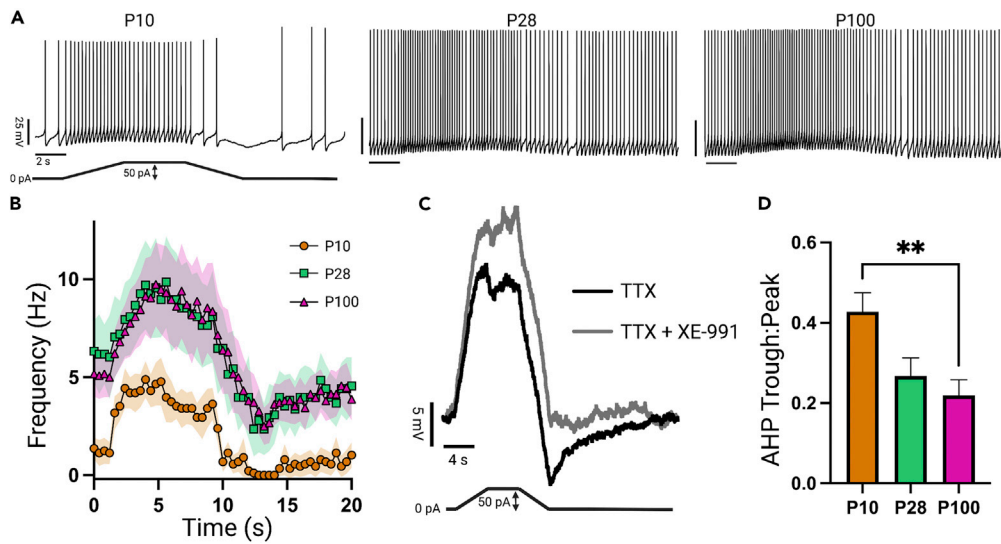


Figure 8. Cell-intrinsic expression of a Kv7.2/3-dependent hyperpolarization is enhanced at P10

(A) Sample whole cell current-clamp recordings of ChIs at P10, P28, and P100 (left to right) given a slowly-ramping 50 pA depolarizing current injection (bottom).

(B) Population average firing frequencies during ramping current injection protocol (P10 n = 17 cells; P28 n = 22; P100 n = 29). Each point represents a 400 ms bin and shaded area represents 95% CI.

(C) Representative current-clamp traces during ramping current injection protocol with TTX (1 μM) applied. Kv7.2/3 blocker XE (25 μM) blocked the afterhyperpolarization (AHP) evoked on termination of current injection.

(D) Summary of comparison by age of AHP evoked at the termination of ramping current injection. AHP is quantified as the ratio of the amplitudes of the trough following injection termination to the peak membrane potential during maximal current injection (trough:peak). Ages compared by one-way ANOVA with Bonferroni correction: $p = 0.0075$, $F(2, 38) = 5.5$; P10 vs. P28 $p = 0.0783$; P10 vs. P100 $p = 0.0061$; P28 vs. P100 $p > 0.999$. P10 n = 10 cells (5 mice); P28 n = 12(5); P100 n = 19(7).

Functional connectivity between long-range excitatory projections and striatal ChIs

It appears that variability in ChI pause responses is due in part to variation in excitatory input strength, in this case from the thalamus. A developmental study using lipophilic dyes to trace long range thalamic axonal projections demonstrated robust striatal penetration of intralaminar thalamic axons in the embryonic period, and that in neonates these axonal projections show complex varicosities that decrease with age (Vercelli et al., 2003). These data are consistent with our finding that thalamic input to ChIs is strongest at P10 and recedes in strength postnatally.

Because of the number and somal proximity of their synapses, thalamic inputs, particularly from the intralaminar nuclei, are thought to exert the most significant excitatory control over ChIs (Lapper and Bolam, 1992; Thomas et al., 2000). Indeed, the study that introduced this *ex vivo* thalamostriatal pause preparation showed that cortical stimulation failed to evoke significant pause responses (Ding et al., 2010), although other studies have utilized cortical stimulation to evoke pauses in ChIs (Doig et al., 2014; Kosillo et al., 2016; Reynolds et al., 2004). Previous studies have shown that in addition to developmental changes in the numbers of excitatory synapses, glutamatergic release probability may be developmentally regulated and differ between cortical and thalamic synapses onto SPNs (Choi and Lovinger, 1997; Ding et al., 2008, 2010). However, we show that thalamic release probability onto ChIs does not significantly change between infancy and adulthood in the context of our stimulation paradigm. By additionally measuring mEPSCs from ChIs over development, we suggest a decrease in the number of excitatory synaptic connections to ChIs between P10 and P100, inclusive of cortical inputs. In contrast, evoked input from cortex onto striatal SPNs increases after birth in mice (Krajeski et al., 2019), although cortex-ChI connectivity over development remains to be studied. "Overproduction" and subsequent refinement of central nervous system synapses by elimination are canonical features of mammalian neurodevelopment (Purves and Lichtman, 1980; Rakic et al., 1986). Future efforts should examine mechanisms by which putative refinement of excitatory input onto ChIs occurs and whether there are deficits in this process, as for example, those found intracortically in models of autism spectrum disorders (ASD) (Hutsler and Zhang, 2010; Tang et al., 2014).

Dopaminergic influence on ChI activity dynamics

ACh release from ChIs elicits striatal dopamine release by activating nAChRs on dopaminergic axons (Kosillo et al., 2016; Threlfell et al., 2012; Zhou et al., 2001). ChIs also robustly express D2Rs, which when activated reduce excitability and attenuate ACh release (Maurice et al., 2004; Stoof and Keibabian, 1982; Yan et al., 1997). Dopamine signaling through ChI D2Rs has been shown in a variety of contexts to facilitate the expression of the ChI pause, as well as membrane dynamics thought to relate to pause expression (Aosaki et al., 1994a; Cover et al., 2019; Ding et al., 2010; Reynolds et al., 2004; Wieland et al., 2014). However, there is a growing appreciation for temporal differences between ChI and dopamine neuron responses to behaviorally-salient stimuli, as well as incomplete dependence of the ChI pause on dopamine signaling in various contexts (Joshua et al., 2008; Martyniuk et al., 2022; Morris et al., 2004; Zhang and Cragg, 2017).

Given our previous demonstration that dopamine release—particularly as facilitated by cholinergic signaling—is drastically attenuated in P10 mice and rapidly develops over the first four postnatal weeks, we asked whether this dependence of the ChI pause on D2R signaling was developmentally determined (Lieberman et al., 2018; McQuirt et al., 2021). Remarkably, we observed no dependence of the ChI pause response at P10 on dopamine signaling. A pair of recent studies manipulating D2R expression in striatal ChIs validates the role of dopamine signaling in mediating the length of cue-induced quiescence in adulthood (Gallo et al., 2022; Martyniuk et al., 2022). However, genetic ablation of D2Rs from ChIs did not fully occlude cue-induced reductions in ACh release and produced no behavioral deficits (Martyniuk et al., 2022). Future work should examine whether developmental insults impact the postnatal acquisition of this D2R-dependence.

Cell-intrinsic biophysical mechanisms for ChI pause generation

Aside from an acute reduction in excitability resulting from D2R stimulation, three prominent candidate cell-intrinsic mechanisms proposed for the generation of ChI pause responses are the hyperpolarization-activated I_h current carried by HCN channels, the sAHP, and the slowly-activating, noninactivating potassium current carried in ChIs by Kv7.2/3 channels (Oswald et al., 2009; Zhang et al., 2018). We sought to uncover whether modulation of these currents had effects on thalamus-driven pause responses and whether these effects were developmentally determined.

Temporally specific recruitment and/or inactivation of I_h would provide parsimonious resolution of the pause mechanism, as HCN channel activity can be potently regulated by D2R signaling (Deng et al., 2007; Lee et al., 2021; Wainger et al., 2001). However, the directionality of I_h effects on pause-related membrane dynamics is unclear, with hypotheses that I_h inactivation causes pause-related hyperpolarizations (Oswald et al., 2009) or instead that these effects were an artifact of chronic hyperpolarization caused by I_h blockade (Zhang et al., 2018). Our data are consistent with a canonical pacemaking role for I_h in striatal ChIs, as blockade of HCN channels resulted in prolonged pauses at P28 and p100. In this case, it appears that removal of I_h -driven depolarization allows for an extended persistence of ChI quiescence, rather than a flattening of membrane responses. The developmental trajectory of the pause response is then consistent with our observation of increasing I_h expression during maturation of striatal ChIs. However, the cellular variability in functional I_h expression does not explain the variation in competency to pause at each age, suggesting that the upstream recruitment of I_h by D2Rs, afferent excitation, or another mechanism may be developmentally dynamic as well as bulk expression of the current.

The sAHP provides an attractive alternative mechanism due to its slow kinetics and particular recruitment after exogenous excitation. Indeed, after a direct depolarizing current injection, ChIs show a pause in firing due to this afterhyperpolarization. It has been unclear, however, whether this relates to the pauses seen *in vivo* and in various reduced preparations using circuit stimulation rather than direct depolarization. By blocking L-type calcium channels—to which the sAHP current is selectively coupled—we reduced the expression of the sAHP with no effect on the significant pause responses at P10, suggesting that thalamic stimulation recruits an alternate mechanism to promote pausing.

Finally, we examined the Kv7.2/3 current, which like the sAHP is a slow outward potassium conductance recruited following significant exogenous excitation. Quantification of both the XE-991-sensitive activation current and afterhyperpolarization driven by ramping depolarization suggested that the functional expression of Kv7.2/3 was highest at P10 and decreased with age. XE-991 incubation significantly downregulated the expression of thalamus-driven ChI pauses at P10—the only manipulation we found to do so—while

having no significant effect at P28 or P100, leading to the conclusion that the enhanced pauses observed at P10 are facilitated by enhanced expression of Kv7.2/3 at this age. The striking developmental decrease in the functional expression of the Kv7.2/3 current is in stark contrast to our previous measures of other conductances characteristic of the striatal ChI, in which we found that functional magnitudes of I_{h} , I_{SK} , I_A , I_{NaP} , and putatively I_{BK} each increase significantly over this developmental time course (McGuirt et al., 2021).

These functional assays of the Kv7.2/3 current are consistent with data from large transcriptomic studies of both the developing mouse and human brain. In mice, Kv7.3 transcript peaks at P4 and then decreases to adult levels (Lein et al., 2007; Thompson et al., 2014). In the human striatum, Kv7.2 expression is highest perinatally and decreases after 1 year of age. Kv7.3 expression is low embryonically and shows two peaks at 1 and 19 years of age before resuming low expression in adulthood (Li et al., 2018). As current is likely most efficiently carried by a Kv7.2/3 heterotetramer (Springer et al., 2021), these data correspond to our functional determination that the Kv7.2/3 current is expressed at its highest levels in the early postnatal period in mice.

Gain of function mutations in the KCNQ channel family cause neonatal seizures, early-onset epileptic encephalopathies, and features of autism spectrum disorders (ASD) (Miceli et al., 2015; Sands et al., 2019; Springer et al., 2021). Given the role of the striatal ChI in promoting behavioral flexibility, and the growing appreciation for striatal function in the expression of ASD symptomatology, future work should probe whether ChI intrinsic physiology—including Kv7.2/3 expression and function—mediates behavioral differences observed in ASD.

Implications and conclusions

Despite early functionality of relevant sensorimotor processes, conditioned aversive and appetitive responses are limited in young rodents and humans (Gee et al., 2018). With maturation comes the ability to learn to recognize and act on a vast set of subtly differentiable cues with a growing repertoire of behavioral responses. It has recently been suggested that ChI pauses are part of a coincidence gate allowing for the expression of certain forms of striatal plasticity (Reynolds et al., 2022). Speculatively, in juveniles, a heightened competency to pause may promote greater permissiveness for plasticity expression, while also reflecting a demand for robust responses to a few salient cues necessary for survival. With development and learning, the computations of the striatal microcircuit are refined, as required by navigation through an environment with complexifying demands. Notably, lesions of ChIs or their thalamic inputs cause deficits in behavioral flexibility and the ability to incorporate new cues, leading to perseverative responses based on previously-learned cues (Aoki et al., 2015; Bradfield et al., 2013). Although additional study will be necessary to elucidate the relationships between ChI activity dynamics and cued behavioral responding over development, these data provide an initial illustration of how functional expression the ChI pause changes postnatally, and identify multiple dependencies of the pause that are differentially engaged during postnatal maturation.

Limitations of the study

As circuit-driven ChI activity dynamics are probed in more model systems and contexts, we think that it is becoming evident that the “ChI pause” is not a singular phenomenon, but rather a convergent result of the multifactorial expression of several mechanistic pathways. Based on our experimental design, our analysis was limited to one strain of ChI pause—namely, the pause initiated by significant innervation from the thalamus. There may be variations in pause generation dependent on the source of innervation that we did not examine that could rely on other candidate pause mechanisms. In addition, there are limitations inherent in the use of *ex vivo* brain slices to study these circuit-driven phenomena. Despite utilizing a slice that retains one particularly salient feature of the striatal microcircuit (thalamostriatal axons), the connectivity and ongoing circuit modulation of the ChI is quite different than *in vivo*, where the ChI pause was first described. Given the technical difficulty of recording from live neonatal rodents, we think this experimental design is well suited to begin to uncover the developmental dynamics of the striatal circuit. However, as genetically-encoded biosensors (for instance, acetylcholine sensors) progress and become quantifiably comparable across developmental time, our ability to answer these questions and their downstream implications will greatly improve.

STAR★METHODS

Detailed methods are provided in the online version of this paper and include the following:

- KEY RESOURCES TABLE

- **RESOURCE AVAILABILITY**
 - Lead contact
 - Materials availability
 - Data and code availability
- **EXPERIMENTAL MODEL AND SUBJECT DETAILS**
 - Mouse lines
- **METHOD DETAILS**
 - Ex vivo thalamostriatal slices
 - Spontaneous firing and thalamostriatal stimulation
 - Voltage clamp experiments
 - Miniature excitatory postsynaptic currents
- **QUANTIFICATION AND STATISTICAL ANALYSIS**

SUPPLEMENTAL INFORMATION

Supplemental information can be found online at <https://doi.org/10.1016/j.isci.2022.105332>.

ACKNOWLEDGMENTS

A.M. was supported by NIDA (F31DA052185). Supported by National Institutes of Health NIDA R01DA007418 (D.S) and the JPB Foundation (D.S). We give special thanks to Ori Lieberman for technical guidance, training, and inspiring initial directions of this project.

AUTHOR CONTRIBUTIONS

Conceptualization, A.M. and D.S.; Methodology, A.M. and I.P.; Investigation, A.M. and I.P.; Formal Analysis, A.M.; Writing—Original Draft, A.M.; Writing—Review/Editing, A.M. and D.S.; Funding Acquisition, A.M. and D.S.; Resources/Supervision, D.S.

DECLARATION OF INTERESTS

The authors declare no competing interests.

Received: February 9, 2022

Revised: August 18, 2022

Accepted: October 10, 2022

Published: November 18, 2022

REFERENCES

- Alleva, E., and D'Udine, B. (1987). Early learning capability in rodents: a review (*Rattus norvegicus* and *Mus Musculus*). *Int. J. Comp. Psychol.* <https://escholarship.org/uc/item/60n077z3>
- Altman, J., and Sudarshan, K. (1975). Postnatal development of locomotion in the laboratory rat. *Anim. Behav.* 23, 896–920. [https://doi.org/10.1016/0003-3472\(75\)90114-1](https://doi.org/10.1016/0003-3472(75)90114-1).
- Aoki, S., Liu, A.W., Zucca, A., Zucca, S., and Wickens, J.R. (2015). Role of striatal cholinergic interneurons in set-shifting in the rat. *J. Neurosci.* 35, 9424–9431. <https://doi.org/10.1523/JNEUROSCI.0490-15.2015>.
- Aosaki, T., Graybiel, A.M., and Kimura, M. (1994a). Effect of the nigrostriatal dopamine system on acquired neural responses in the striatum of behaving monkeys. *Science* 265, 412–415. <https://doi.org/10.1126/science.8023166>.
- Aosaki, T., Kimura, M., and Graybiel, A.M. (1995). Temporal and spatial characteristics of tonically active neurons of the primate's striatum. *J. Neurophysiol.* 73, 1234–1252. <https://doi.org/10.1152/jn.1995.73.3.1234>.
- Aosaki, T., Tsubokawa, H., Ishida, A., Watanabe, K., Graybiel, A.M., and Kimura, M. (1994b). Responses of tonically active neurons in the primate's striatum undergo systematic changes during behavioral sensorimotor conditioning. *J. Neurosci.* 14, 3969–3984.
- Bolam, J.P., Wainer, B.H., and Smith, A.D. (1984). Characterization of cholinergic neurons in the rat neostriatum. A combination of choline acetyltransferase immunocytochemistry, Golgi-impregnation and electron microscopy. *Neuroscience* 12, 711–718. [https://doi.org/10.1016/0306-4522\(84\)90165-9](https://doi.org/10.1016/0306-4522(84)90165-9).
- Braak, H., and Braak, E. (1982). Neuronal types in the striatum of man. *Cell Tissue Res.* 227, 319–342. <https://doi.org/10.1007/BF00210889>.
- Bradfield, L.A., Bertran-Gonzalez, J., Chieng, B., and Balleine, B.W. (2013). The thalamostriatal pathway and cholinergic control of goal-directed action: interlacing new with existing learning in the striatum. *Neuron* 79, 153–166. <https://doi.org/10.1016/j.neuron.2013.04.039>.
- Bulut, F., and Altman, J. (1974). Spatial and tactile discrimination learning in infant rats motivated by homing. *Dev. Psychobiol.* 7, 465–473. <https://doi.org/10.1002/dev.420070510>.
- Choi, S., and Lovinger, D.M. (1997). Decreased probability of neurotransmitter release underlies striatal long-term depression and postnatal development of corticostriatal synapses. *Proc. Natl. Acad. Sci. USA* 94, 2665–2670. <https://doi.org/10.1073/pnas.94.6.2665>.
- Choi, S.J., Ma, T.C., Ding, Y., Cheung, T., Joshi, N., Sulzer, D., Mosharov, E.V., and Kang, U.J. (2020). Alterations in the intrinsic properties of striatal cholinergic interneurons after dopamine lesion and chronic L-DOPA. *Elife* 9, e56920. <https://doi.org/10.7554/eLife.56920>.
- Cover, K.K., Gyawali, U., Kerkhoff, W.G., Patton, M.H., Mu, C., White, M.G., Marquardt, A.E., Roberts, B.M., Cheer, J.F., and Mathur, B.N. (2019). Activation of the rostral intralaminar thalamus drives reinforcement through striatal dopamine release. *Cell Rep.* 26, 1389–1398.e3. <https://doi.org/10.1016/j.celrep.2019.01.044>.

- Deng, P., Zhang, Y., and Xu, Z.C. (2007). Involvement of I(h) in dopamine modulation of tonic firing in striatal cholinergic interneurons. *J. Neurosci.* 27, 3148–3156. <https://doi.org/10.1523/JNEUROSCI.5535-06.2007>.
- Ding, J., Peterson, J.D., and Surmeier, D.J. (2008). Corticostriatal and thalamostriatal synapses have distinctive properties. *J. Neurosci.* 28, 6483–6492. <https://doi.org/10.1523/JNEUROSCI.0435-08.2008>.
- Ding, J.B., Guzman, J.N., Peterson, J.D., Goldberg, J.A., and Surmeier, D.J. (2010). Thalamic gating of corticostriatal signaling by cholinergic interneurons. *Neuron* 67, 294–307. <https://doi.org/10.1016/j.neuron.2010.06.017>.
- Doig, N.M., Magill, P.J., Apicella, P., Bolam, J.P., and Sharott, A. (2014). Cortical and thalamic excitation mediate the multiphasic responses of striatal cholinergic interneurons to motivationally salient stimuli. *J. Neurosci.* 34, 3101–3117. <https://doi.org/10.1523/JNEUROSCI.4627-13.2014>.
- Fox, W.M. (1965). Reflex-ontogeny and behavioural development of the mouse. *Anim. Behav.* 13, 234–241. [https://doi.org/10.1016/0003-3472\(65\)90041-2](https://doi.org/10.1016/0003-3472(65)90041-2).
- Gallo, E.F., Greenwald, J., Yeisley, J., Teboul, E., Martyniuk, K.M., Villarin, J.M., Li, Y., Javitch, J.A., Balsam, P.D., and Kellendonk, C. (2022). Dopamine D2 receptors modulate the cholinergic pause and inhibitory learning. *Mol. Psychiatr.* 27, 1502–1514. <https://doi.org/10.1038/s41380-021-01364-y>.
- Gee, D.G., Bath, K.G., Johnson, C.M., Meyer, H.C., Murty, V.P., van den Bos, W., and Hartley, C.A. (2018). Neurocognitive development of motivated behavior: dynamic changes across childhood and adolescence. *J. Neurosci.* 38, 9433–9445. <https://doi.org/10.1523/JNEUROSCI.1674-18.2018>.
- Gerfen, C.R., and Surmeier, D.J. (2011). Modulation of striatal projection systems by dopamine. *Annu. Rev. Neurosci.* 34, 441–466. <https://doi.org/10.1146/annurev-neuro-061010-113641>.
- Goldberg, J.A., and Wilson, C.J. (2005). Control of spontaneous firing patterns by the selective coupling of calcium currents to calcium-activated potassium currents in striatal cholinergic interneurons. *J. Neurosci.* 25, 10230–10238. <https://doi.org/10.1523/JNEUROSCI.2734-05.2005>.
- Hall, W.G., Cramer, C.P., and Blass, E.M. (1977). Ontogeny of suckling in rats: transitions toward adult ingestion. *J. Comp. Physiol. Psychol.* 91, 1141–1155. <https://doi.org/10.1037/h0077388>.
- Howe, W.M., Young, D.A., Bekheet, G., and Kozak, R. (2016). Nicotinic receptor subtypes differentially modulate glutamate release in the dorsal medial striatum. *Neurochem. Int.* 100, 30–34. <https://doi.org/10.1016/j.neuint.2016.08.009>.
- Hutsler, J.J., and Zhang, H. (2010). Increased dendritic spine densities on cortical projection neurons in autism spectrum disorders. *Brain Res.* 1309, 83–94. <https://doi.org/10.1016/j.brainres.2009.09.120>.
- Joshua, M., Adler, A., Mitelman, R., Vaadia, E., and Bergman, H. (2008). Midbrain dopaminergic neurons and striatal cholinergic interneurons encode the difference between reward and aversive events at different epochs of probabilistic classical conditioning trials. *J. Neurosci.* 28, 11673–11684. <https://doi.org/10.1523/JNEUROSCI.3839-08.2008>.
- Kemp, J.M., and Powell, T.P. (1971). The structure of the caudate nucleus of the cat: light and electron microscopy. *Philos. Trans. R. Soc. Lond. B Biol. Sci.* 262, 383–401. <https://doi.org/10.1098/rstb.1971.0102>.
- Khandelwal, N., Cavalier, S., Rybalchenko, V., Kulkarni, A., Anderson, A.G., Konopka, G., and Gibson, J.R. (2021). FOXP1 negatively regulates intrinsic excitability in D2 striatal projection neurons by promoting inwardly rectifying and leak potassium currents. *Mol. Psychiatr.* 26, 1761–1774. <https://doi.org/10.1038/s41380-020-00995-x>.
- Kharkwal, G., Bami-Cherrier, K., Lizardi-Ortiz, J.E., Nelson, A.B., Ramos, M., Del Barrio, D., Sulzer, D., Kreitzer, A.C., and Borrelli, E. (2016). Parkinsonism driven by antipsychotics originates from dopaminergic control of striatal cholinergic interneurons. *Neuron* 91, 67–78. <https://doi.org/10.1016/j.neuron.2016.06.014>.
- Kosillo, P., Zhang, Y.-F., Threlfell, S., and Cragg, S.J. (2016). Cortical control of striatal dopamine transmission via striatal cholinergic interneurons. *Cereb. Cortex* 26, 4160–4169. <https://doi.org/10.1093/cercor/bhw252>.
- Kozorovitskiy, Y., Peixoto, R., Wang, W., Saunders, A., and Sabatini, B.L. (2015). Neuromodulation of excitatory synaptogenesis in striatal development. *Elife* 4, e10111. <https://doi.org/10.7554/eLife.10111>.
- Kozorovitskiy, Y., Saunders, A., Johnson, C.A., Lowell, B.B., and Sabatini, B.L. (2012). Recurrent network activity drives striatal synaptogenesis. *Nature* 485, 646–650. <https://doi.org/10.1038/nature11052>.
- Krajcski, R.N., Macey-Dare, A., van Heusden, F., Ebrahimjee, F., and Ellender, T.J. (2019). Dynamic postnatal development of the cellular and circuit properties of striatal D1 and D2 spiny projection neurons. *J. Physiol.* 597, 5265–5293. <https://doi.org/10.1113/JP278416>.
- Lapper, S.R., and Bolam, J.P. (1992). Input from the frontal cortex and the parafascicular nucleus to cholinergic interneurons in the dorsal striatum of the rat. *Neuroscience* 51, 533–545. [https://doi.org/10.1016/0306-4522\(92\)90293-b](https://doi.org/10.1016/0306-4522(92)90293-b).
- Lee, J., Weinberger, M., Kawahara, Y., Cheng, J., Umschweif, G., Medrihan, L., Flajolet, M., Nishi, A., and Sagi, Y. (2021). HC2N1 in cholinergic interneurons of the nucleus accumbens mediates reward response. Preprint at bioRxiv. <https://doi.org/10.1101/2021.09.21.460269>.
- Lein, E.S., Hawrylycz, M.J., Ao, N., Ayres, M., Bensinger, A., Bernard, A., Boe, A.F., Boguski, M.S., Brockway, K.S., Byrnes, E.J., et al. (2007). Genome-wide atlas of gene expression in the adult mouse brain. *Nature* 445, 168–176. <https://doi.org/10.1038/nature05453>.
- Lieberman, O.J., Frier, M.D., McGuirt, A.F., Griffey, C.J., Rafikian, E., Yang, M., Yamamoto, A., Borgkvist, A., Santini, E., and Sulzer, D. (2020). Cell-type-specific regulation of neuronal intrinsic excitability by macroautophagy. *Elife* 9, e50843. <https://doi.org/10.7554/eLife.50843>.
- Lieberman, O.J., McGuirt, A.F., Mosharov, E.V., Pigulevskiy, I., Hobson, B.D., Choi, S., Frier, M.D., Santini, E., Borgkvist, A., and Sulzer, D. (2018). Dopamine triggers the maturation of striatal spiny projection neuron excitability during a critical period. *Neuron* 99, 540–554.e4. <https://doi.org/10.1016/j.neuron.2018.06.044>.
- Li, M., Santpere, G., Imamura Kawasawa, Y., Evgrafov, O.V., Gulden, F.O., Pochareddy, S., Sunkin, S.M., Li, Z., Shin, Y., et al.; BrainSpan Consortium; PsychENCODE Consortium; PsychENCODE Developmental Subgroup (2018). Integrative functional genomic analysis of human brain development and neuropsychiatric risks. *Science* 362, eaat7615. <https://doi.org/10.1126/science.aat7615>.
- Martyniuk, K.M., Torres-Herrera, A., Lowes, D.C., Rubinstein, M., Labouesse, M.A., and Kellendonk, C. (2022). Dopamine D2Rs coordinate cue-evoked changes in striatal acetylcholine levels. *Elife* 11, e76111. <https://doi.org/10.7554/eLife.76111>.
- Matsumoto, N., Minamimoto, T., Graybiel, A.M., and Kimura, M. (2001). Neurons in the thalamic CM-Pf complex supply striatal neurons with information about behaviorally significant sensory events. *J. Neurophysiol.* 85, 960–976. <https://doi.org/10.1152/jn.2001.85.2.960>.
- Maurice, N., Mercer, J., Chan, C.S., Hernandez-Lopez, S., Held, J., Tkatch, T., and Surmeier, D.J. (2004). D2 dopamine receptor-mediated modulation of voltage-dependent Na⁺ channels reduces autonomous activity in striatal cholinergic interneurons. *J. Neurosci.* 24, 10289–10301. <https://doi.org/10.1523/JNEUROSCI.2155-04.2004>.
- McGuirt, A.F., Post, M.R., Pigulevskiy, I., Sulzer, D., and Lieberman, O.J. (2021). Coordinated postnatal maturation of striatal cholinergic interneurons and dopamine release dynamics in mice. *J. Neurosci.* 41, 3597–3609. <https://doi.org/10.1523/JNEUROSCI.0755-20.2021>.
- Miceli, F., Soldovieri, M.V., Ambrosino, P., De Maria, M., Migliore, M., Migliore, R., and Tagliatela, M. (2015). Early-onset epileptic encephalopathy caused by gain-of-function mutations in the voltage sensor of Kv7.2 and Kv7.3 potassium channel subunits. *J. Neurosci.* 35, 3782–3793. <https://doi.org/10.1523/JNEUROSCI.4423-14.2015>.
- Morris, G., Arkadir, D., Nevet, A., Vaadia, E., and Bergman, H. (2004). Coincident but distinct messages of midbrain dopamine and striatal tonically active neurons. *Neuron* 43, 133–143. <https://doi.org/10.1016/j.neuron.2004.06.012>.
- n.d. Psth Narayan, R.. MATLAB central file exchange. <https://www.mathworks.com/matlabcentral/fileexchange/14745-psth>.
- Oldenburg, I.A., and Ding, J.B. (2011). Cholinergic modulation of synaptic integration and dendritic excitability in the striatum. *Curr. Opin. Neurobiol.* 21, 425–432. <https://doi.org/10.1016/j.conb.2011.04.004>.
- Oswald, M.J., Oorschot, D.E., Schulz, J.M., Lipski, J., and Reynolds, J.N.J. (2009). IH current

generates the afterhyperpolarisation following activation of subthreshold cortical synaptic inputs to striatal cholinergic interneurons. *J. Physiol.* 587, 5879–5897. <https://doi.org/10.1113/jphysiol.2009.177600>.

Peixoto, R.T., Chantranupong, L., Hakim, R., Levasseur, J., Wang, W., Merchant, T., Gorman, K., Budnik, B., and Sabatini, B.L. (2019). Abnormal striatal development underlies the early onset of behavioral deficits in Shank3B^{-/-} mice. *Cell Rep.* 29, 2016–2027.e4. <https://doi.org/10.1016/j.celrep.2019.10.021>.

Peixoto, R.T., Wang, W., Croney, D.M., Kozorovitskiy, Y., and Sabatini, B.L. (2016). Early hyperactivity and precocious maturation of corticostriatal circuits in Shank3B^{-/-} mice. *Nat. Neurosci.* 19, 716–724. <https://doi.org/10.1038/nn.4260>.

Purves, D., and Lichtman, J.W. (1980). Elimination of synapses in the developing nervous system. *Science* 210, 153–157. <https://doi.org/10.1126/science.7414326>.

Rakic, P., Bourgeois, J.P., Eckenhoff, M.F., Zecevic, N., and Goldman-Rakic, P.S. (1986). Concurrent overproduction of synapses in diverse regions of the primate cerebral cortex. *Science* 232, 232–235. <https://doi.org/10.1126/science.3952506>.

Reynolds, J.N.J., Avisati, R., Dodson, P.D., Fisher, S.D., Oswald, M.J., Wickens, J.R., and Zhang, Y.-F. (2022). Coincidence of cholinergic pauses, dopaminergic activation and depolarisation of spiny projection neurons drives synaptic plasticity in the striatum. *Nat. Commun.* 13, 1296. <https://doi.org/10.1038/s41467-022-28950-0>.

Reynolds, J.N.J., Hyland, B.I., and Wickens, J.R. (2004). Modulation of an afterhyperpolarization by the substantia nigra induces pauses in the tonic firing of striatal cholinergic interneurons. *J. Neurosci.* 24, 9870–9877. <https://doi.org/10.1523/JNEUROSCI.3225-04.2004>.

Rice, M.E., and Cragg, S.J. (2004). Nicotine amplifies reward-related dopamine signals in striatum. *Nat. Neurosci.* 7, 583–584. <https://doi.org/10.1038/nn1244>.

Sanchez, G., Rodriguez, M.J., Pomata, P., Rela, L., and Murer, M.G. (2011). Reduction of an afterhyperpolarization current increases excitability in striatal cholinergic interneurons in rat parkinsonism. *J. Neurosci.* 31, 6553–6564. <https://doi.org/10.1523/JNEUROSCI.6345-10.2011>.

Sands, T.T., Miceli, F., Lesca, G., Beck, A.E., Sadleir, L.G., Arrington, D.K., Schönewolf-Greulich, B., Moutton, S., Lauritano, A., Nappi, P., et al. (2019). Autism and developmental disability caused by KCNQ3 gain-of-function variants. *Ann. Neurol.* 86, 181–192. <https://doi.org/10.1002/ana.25522>.

Saunders, A., Macosko, E.Z., Wysoker, A., Goldman, M., Krienen, F.M., de Rivera, H., Bien, E., Baum, M., Bortolin, L., Wang, S., et al. (2018).

Molecular diversity and specializations among the cells of the adult mouse brain. *Cell* 174, 1015–1030.e16. <https://doi.org/10.1016/j.cell.2018.07.028>.

Shen, W., Hamilton, S.E., Nathanson, N.M., and Surmeier, D.J. (2005). Cholinergic suppression of KCNQ channel currents enhances excitability of striatal medium spiny neurons. *J. Neurosci.* 25, 7449–7458. <https://doi.org/10.1523/JNEUROSCI.1381-05.2005>.

Smeal, R.M., Gaspar, R.C., Keefe, K.A., and Wilcox, K.S. (2007). A rat brain slice preparation for characterizing both thalamostriatal and corticostriatal afferents. *J. Neurosci. Methods* 159, 224–235. <https://doi.org/10.1016/j.jneumeth.2006.07.007>.

Smith, Y., Raju, D.V., Pare, J.-F., and Sidibe, M. (2004). The thalamostriatal system: a highly specific network of the basal ganglia circuitry. *Trends Neurosci.* 27, 520–527. <https://doi.org/10.1016/j.tins.2004.07.004>.

Springer, K., Varghese, N., and Tzingounis, A.V. (2021). Flexible stoichiometry: implications for KCNQ2- and KCNQ3-associated neurodevelopmental disorders. *Dev. Neurosci.* 43, 191–200. <https://doi.org/10.1159/000515495>.

Stoof, J.C., and Keibarian, J.W. (1982). Independent in vitro regulation by the D-2 dopamine receptor of dopamine-stimulated efflux of cyclic AMP and K⁺-stimulated release of acetylcholine from rat neostriatum. *Brain Res.* 250, 263–270. [https://doi.org/10.1016/0006-8993\(82\)90420-6](https://doi.org/10.1016/0006-8993(82)90420-6).

Tang, G., Gudsruk, K., Kuo, S.-H., Cotrina, M.L., Rosoklija, G., Sosunov, A., Sonders, M.S., Kanter, E., Castagna, C., Yamamoto, A., et al. (2014). Loss of mTOR-dependent macroautophagy causes autistic-like synaptic pruning deficits. *Neuron* 83, 1131–1143. <https://doi.org/10.1016/j.neuron.2014.07.040>.

Tanimura, A., Lim, S.A.O., Aceves Buendia, J.d.J., Goldberg, J.A., and Surmeier, D.J. (2016). Cholinergic interneurons amplify corticostriatal synaptic responses in the Q175 model of huntington's disease. *Front. Syst. Neurosci.* 10, 102. <https://doi.org/10.3389/fnsys.2016.00102>.

Thomas, T.M., Smith, Y., Levey, A.I., and Hersch, S.M. (2000). Cortical inputs to m2-immunoreactive striatal interneurons in rat and monkey. *Synapse* 37, 252–261. [https://doi.org/10.1002/1098-2396\(20000915\)37:4<252::AID-SYN2>3.0.CO;2-A](https://doi.org/10.1002/1098-2396(20000915)37:4<252::AID-SYN2>3.0.CO;2-A).

Thompson, C.L., Ng, L., Menon, V., Martinez, S., Lee, C.-K., Glattfelder, K., Sunkin, S.M., Henry, A., Lau, C., Dang, C., et al. (2014). A high-resolution spatiotemporal atlas of gene expression of the developing mouse brain. *Neuron* 83, 309–323. <https://doi.org/10.1016/j.neuron.2014.05.033>.

Threlfell, S., Lalic, T., Platt, N.J., Jennings, K.A., Deisseroth, K., and Cragg, S.J. (2012). Striatal dopamine release is triggered by synchronized activity in cholinergic interneurons.

Neuron 75, 58–64. <https://doi.org/10.1016/j.neuron.2012.04.038>.

Vercelli, A., Marini, G., and Tredici, G. (2003). Anatomical organization of the telencephalic connections of the parafascicular nucleus in adult and developing rats. *Eur. J. Neurosci.* 18, 275–289. <https://doi.org/10.1046/j.1460-9568.2003.02743.x>.

Wainger, B.J., DeGennaro, M., Santoro, B., Siegelbaum, S.A., and Tibbs, G.R. (2001). Molecular mechanism of cAMP modulation of HCN pacemaker channels. *Nature* 411, 805–810. <https://doi.org/10.1038/35081088>.

Wang, H.S., Pan, Z., Shi, W., Brown, B.S., Wymore, R.S., Cohen, I.S., Dixon, J.E., and McKinnon, D. (1998). KCNQ2 and KCNQ3 potassium channel subunits: molecular correlates of the M-channel. *Science* 282, 1890–1893. <https://doi.org/10.1126/science.282.5395.1890>.

Wieland, S., Du, D., Oswald, M.J., Parlato, R., Köhr, G., and Kelsch, W. (2014). Phasic dopaminergic activity exerts fast control of cholinergic interneuron firing via sequential NMDA, D2, and D1 receptor activation. *J. Neurosci.* 34, 11549–11559. <https://doi.org/10.1523/JNEUROSCI.1175-14.2014>.

Wilson, C.J., and Goldberg, J.A. (2006). Origin of the slow afterhyperpolarization and slow rhythmic bursting in striatal cholinergic interneurons. *J. Neurophysiol.* 95, 196–204. <https://doi.org/10.1152/jn.00630.2005>.

Wilson, C.J. (2005). The mechanism of intrinsic amplification of hyperpolarizations and spontaneous bursting in striatal cholinergic interneurons. *Neuron* 45, 575–585. <https://doi.org/10.1016/j.neuron.2004.12.053>.

Yan, Z., Song, W.J., and Surmeier, J. (1997). D2 dopamine receptors reduce N-type Ca²⁺ currents in rat neostriatal cholinergic interneurons through a membrane-delimited, protein-kinase-C-insensitive pathway. *J. Neurophysiol.* 77, 1003–1015. <https://doi.org/10.1152/jn.1997.77.2.1003>.

Zhang, H., and Sulzer, D. (2004). Frequency-dependent modulation of dopamine release by nicotine. *Nat. Neurosci.* 7, 581–582. <https://doi.org/10.1038/nn1243>.

Zhang, Y.-F., and Cragg, S.J. (2017). Pauses in striatal cholinergic interneurons: what is revealed by their common themes and variations? *Front. Syst. Neurosci.* 11, 80. <https://doi.org/10.3389/fnsys.2017.00080>.

Zhang, Y.-F., Reynolds, J.N.J., and Cragg, S.J. (2018). Pauses in cholinergic interneuron activity are driven by excitatory input and delayed rectification, with dopamine modulation. *Neuron* 98, 918–925.e3. <https://doi.org/10.1016/j.neuron.2018.04.027>.

Zhou, F.M., Liang, Y., and Dani, J.A. (2001). Endogenous nicotinic cholinergic activity regulates dopamine release in the striatum. *Nat. Neurosci.* 4, 1224–1229. <https://doi.org/10.1038/nn769>.

STAR★METHODS

KEY RESOURCES TABLE

REAGENT or RESOURCE	SOURCE	IDENTIFIER
Chemicals, peptides, and recombinant proteins		
tetrodotoxin citrate (TTX)	Tocris	Cat#:1069
ZD7288 (ZD)	Tocris	Cat#:1000
picrotoxin (PTX)	Tocris	Cat#:1128
XE-991 dihydrochloride (XE)	Tocris	Cat#: 2000
(S)-(-)-sulpiride	Tocris	Cat#: 0895
QX 314 bromide	Tocris	Cat#:1014
Nifedipine	Tocris	Cat#: 1075
Experimental models: Organisms/strains		
C57BL/6J mouse	Jackson Laboratory	JAX strain# 000664
Software and algorithms		
Pclamp10	Molecular Devices	RRID:SCR_011323
Clampfit 10.7	Molecular Devices	RRID:SCR_011323
Matlab 2021b	MathWorks	RRID:SCR_001622
Prism 9	GraphPad	RRID:SCR_002798
BioRender	biorender.com	RRID:SCR_018361

RESOURCE AVAILABILITY

Lead contact

Further information and requests for resources and reagents should be directed to and will be fulfilled by the lead contact, David Sulzer (ds43@cumc.columbia.edu).

Materials availability

This study did not generate new unique reagents.

Data and code availability

- All data reported in this paper will be shared by the [lead contact](#) upon request
- This paper does not report original code
- Any additional information required to reanalyze the data reported in this paper is available from the [lead contact](#) upon request.

EXPERIMENTAL MODEL AND SUBJECT DETAILS

Mouse lines

C57Bl6J breeder pairs were obtained initially from Jackson Laboratories (Bar Harbor, ME). Mice were housed in same-sex groups of 2–5 on a 12-hour light/dark cycle with *ad libitum* food and water availability. Breeding pairs were checked daily for pregnancies and new litters. Male and female mice were used at P10, P28, or P100. Mice were used for experiments on the specified postnatal day (± 1 day) for all P10 and P28 groups, and (± 10 days) for P100 groups. All experimental procedures were approved by the Columbia University Institutional Animal Care and Use Committee and followed guidelines established in the NIH Guide for the Care and Use of Laboratory Animals. We found no differences between sexes and the data combine male and female mice.

METHOD DETAILS

Ex vivo thalamostriatal slices

To generate acute brain slices, mice underwent rapid cervical dislocation and the brain was placed in ice-cold cutting buffer (in mM): 10 NaCl, 2.5 KCl, 25 NaHCO₃, 0.5 CaCl₂, 7 MgCl₂, 1.25 NaH₂PO₄, 180 sucrose, 10 glucose bubbled with 95% O₂/5% CO₂ to pH 7.4. Angled horizontal thalamostriatal slices were generated as described in (Ding et al., 2010). The basal surface of the brain was affixed to an agarose wedge (20° from horizontal; rostral end pointing down) on the cutting stage of a Leica vibratome (VT1200S). 300 μm slices were collected and incubated at 34°C for 30 min in artificial cerebrospinal fluid (ACSF) (in mM): 125 NaCl, 2.5 KCl, 25 NaHCO₃, 2 CaCl₂, 1 MgCl₂, 1.25 NaH₂PO₄ and 10 glucose bubbled with 95% O₂/5% CO₂ to pH 7.4. Slices were then removed to room temperature and rested for 30 min before recording for a maximum of 4 hours.

Spontaneous firing and thalamostriatal stimulation

For recording, slices were transferred to a recording chamber superfused with oxygenated ACSF maintained at 34°C. For stimulation of thalamostriatal axons, a bipolar tungsten concentric electrode (2–3 μm tip diameter) was placed onto the lateral edge of the thalamus/internal capsule (Figure 1A). ChIs were identified based on the large soma size under IR/DIC optics using a 40X water immersion objective. Liquid junction potential was not corrected. Data were acquired with Clampex 10 software (Molecular Devices, San Jose, CA) using an Axopatch 200B amplifier (Molecular Devices), digitized using a Digidata 1440A (Molecular Devices) at 10 kHz and filtered at 5 kHz.

Cell-attached and whole cell recordings were accomplished using glass pipettes (2–5 MΩ) filled with internal solution (in mM): 115 potassium gluconate, 20 KCl, 20 HEPES, 1 MgCl₂, 2 MgATP, 0.2 NaGTP adjusted to pH 7.25 with KOH, osmolarity 285 mOsm (Choi et al., 2020). Spontaneous firing was verified in cell-attached voltage-clamp recording after a giga-ohm seal was achieved. Subsequently, also in the cell-attached configuration, 10 sweeps of the 10 s pause protocol were run, wherein a train stimulus (10 pulses x 200 μs x 400 μA x 50 Hz) was delivered at 2 s. To calculate the pause score (PS), for each sweep, the average pre-stimulus frequency and the instantaneous frequency following the stimulus were collected. The ratio of the cell average of pre:post frequencies was defined as the pause score. Significance was determined by a paired t-test comparing pre- and post-stimulation values.

Voltage clamp experiments

I_h and Kv7.2/3 currents (Figures 5 and 7) were characterized in the whole-cell voltage-clamp configuration. I_h was quantified as reported in (Choi et al., 2020). Hyperpolarizing steps (–60 and –70 mV) from holding potential (–60 mV) were held for 1 s and the current difference across the voltage step was quantified. We verified that this current was sensitive to the I_h-blocker ZD7288 (1 μM) (Figure 5B). The reported current (Figure 5A) is derived from the –60 mV voltage step. Kv7.2/3 potassium current was identified as the slowly-developing XE-991-sensitive component of the current evoked by depolarizing steps (+10 to +70 mV) from a holding potential of –90 mV, as previously published (Shen et al., 2005). Recordings of the Kv7.2/3 activation current were performed in the presence of TTX (1 μM) to block action potentials as well as ZD7288 (1 μM) to block I_h. XE-991 (25 μM), a selective inhibitor of Kv7.2/3 channels, was bath applied for 10–15 minutes after initial recording, and the activation current magnitude was reported as the difference in current at the end of the voltage step before and after drug application (Shen et al., 2005). Cells with >20% change in input resistance during XE application were discarded from analysis.

Miniature excitatory postsynaptic currents

Postsynaptic glutamatergic currents (mEPSCs) were recorded in the whole-cell voltage-clamp configuration following application of picrotoxin (50 μM) to inhibit GABA_A mediated currents and tetrodotoxin (TTX) (1 μM) to block spontaneous firing in the slice. Cesium methylsulfonate (CsMeSO₃) based internal solution contained (in mM) 120 CsMeSO₃, 5 NaCl, 10 HEPES, 1.1 EGTA, 2 Mg²⁺-ATP, 0.3 Na-GTP, 2 Na-ATP, and 5 QX314 (pH = 7.4; approx. 285 mOsm). Cells were recorded for 2 minutes at a holding potential of –60mV and mEPSCs were detected and analyzed using the ClampFit 10 program (Molecular Devices).

QUANTIFICATION AND STATISTICAL ANALYSIS

Electrophysiology data were analyzed offline using Clampfit 10 (Molecular Devices, Sunnyvale, California). Statistical analysis was conducted in GraphPad Prism 9 (La Jolla, CA). PSTH plots were generated in Matlab

(Mathworks) using (Narayan, n.d.) and concatenated to calculate error bounds using a custom Matlab script. All bar graphs show the mean \pm standard error of the mean. Comparisons of PS used nonparametric statistical tests. For one variable (e.g., PS) among >2 groups, a Kruskal-Wallis analysis of variance was used followed by Dunn's multiple comparison test. For two variables (PS and pharmacological manipulation) compared versus age, multiple Mann-Whitney U tests were used, followed by a Bonferroni-Dunn correction. Dependent measures assumed to be normally distributed (e.g., current amplitudes, firing rates) were analyzed by one- or two-way ANOVA. Cumulative distributions of mEPSC frequency were analyzed by Kolmogorov-Smirnov test. Group sizes were preliminarily determined based on previous similar studies (Lieberman et al., 2018; McGuirt et al., 2021). Figure panels were created in GraphPad Prism 9 and compiled using BioRender.com; schematics in Figure 1A and graphical abstract partially adapted from BioRender "patch pipette (with amplifier circuit)" and neuronal templates.